



Modelling 3D permeability distribution in alluvial fans using facies architecture and geophysical acquisitions

Lin Zhu ¹, Huili Gong ¹, Zhenxue Dai ², Gaoxuan Guo ³, Pietro Teatini ⁴

¹College of Resource Environment and Tourism, Capital Normal University, Laboratory Cultivation Base of Environment Process and Digital Simulation, Beijing, China

²Earth and Environmental Sciences Division, Los Alamos National Laboratory, Los Alamos, New Mexico, United States

³ Beijing Institute of Hydrogeology and Engineering Geology, Beijing, China

⁴ Department of Civil, Environmental and Architectural Engineering, University of Padova, Italy

Correspondence to: Lin Zhu hi-zhulin@163.com; Huili Gong gonghl@263.com

Abstract. Alluvial fans are highly heterogeneous due to complex depositional processes, which make difficult to characterize the spatial distribution of the hydraulic conductivity K . An original methodology is developed to identify the spatial statistical parameters (mean, variance, correlation range) of the hydraulic conductivity in a three-dimensional setting by using geological and geophysical data. The Chaobai River alluvial fan in the Beijing Plain, China, is used as an example to test the proposed approach. Due to the non-stationary property of the K distribution in the alluvial fan, a multi-zone parameterization approach is applied to analyze the conductivity statistical properties of different hydrofacies in the various zones. The composite variance in each zone is computed to describe the evolution of the conductivity along the flow direction. Consistently with the scales of the sedimentary transport energy, the results show that conductivity variances of fine sand, medium-coarse sand, and gravel decrease from the upper (Zone 1) to the lower (Zone 3) portion along the flow direction. In Zone 1, sediments were moved by higher-energy flooding, which induces bad sorting and larger conductivity variances. The composite variance confirms this feature with statistically different facies from Zone 1 to Zone 3. The results of this study provide insights to improve our understanding on conductivity heterogeneity and a method for characterizing the spatial distribution of K in alluvial fans.



1 Introduction

Alluvial fans usually house valuable groundwater resources because of significant water storage and favorable recharge conditions. Sedimentary processes forming alluvial fans are responsible for their complex long-term evolution. Usually, the coarsest material (gravel) is deposited in the upper fan, with the gravel passing into sand in the middle of the fan and then into silt and clay in the tail. A high heterogeneity characterizes the deposit distribution because of the shifting over time of the sediment-transporting streams (Zappa et al., 2006).

Conductivity distributions in alluvial fans can be assigned according to the various hydrofacies simulated by conditional indicator geostatistical methods (Eggleson and Rojstaczer 1998; Ritzi et al., 2000, 2004; Proce et al., 2004; Dai et al., 2005; Harp et al., 2008; Hinnell et al., 2010; Soltanian et al., 2015; Zhu et al., 2015a). However, the geostatistical methods require the stationary assumption, i.e. the distribution of the volumetric proportions and correlation lengths of hydrofacies converge to their mean values in the simulation domain. The hydrofacies and hydraulic conductivity (K) distributions in alluvial fans are generally non-stationary (Weissmann and Fogg, 1999; Anderson, 2007; Zhu et al., 2016a). Hence, the use of these methods may cause large characterization errors and add significant uncertainty to the predictions achieved by groundwater flow and contaminant transport models (Eggleson and Rojstaczer 1998; Irving and Singha 2010; Dai et al., 2014a). Zhu et al., (2016a) adopted a local-stationary assumption by dividing the alluvial fan into three zones along the flow direction of the Chaobai River, China. The zones were properly detected based on the statistical facies distribution. Then, the indicator simulation method was applied to each zone and the simulated hydrofacies distribution in the three zones was used to guide modelling the K distribution.



49 Hydraulic conductivity of granular deposits generally varies with grain size, porosity, and sorting.
50 Traditional methods for K estimate, e.g. well test, permeameter measurements, and grain-size analyses
51 (Niwas et al., 2011), are very expensive, time-consuming, and make difficult to provide representative
52 and sufficient field data for addressing spatial variations of conductivity. Recently, data fusion techniques
53 have been developed for coupled inversion of multi-source data to estimate K distributions for
54 groundwater numerical modeling. Geophysical data (such as surface electric resistivity and various
55 logging data) are relatively inexpensive and can provide considerable information for characterizing
56 subsurface heterogeneous properties (Hubbard et al., 2001; Yeh et al., 2002; Dai et al., 2004a; Morin
57 2006; Sikandar et al., 2010; Bevington et al., 2016). Electric resistivity data have been proven useful to
58 derive sediment porosity distributions (Niwas and Singhal 1985; Niwas et al., 2011; Niwas and Celik
59 2012; Zhu et al., 2016b).

60 This study proposes an integrated approach to reconstruct the three-dimensional configuration of
61 conductivity in alluvial fans by combining the hydrofacies spatial heterogeneity provided by a multi-zone
62 transition probability model with hydrogeological and hydrogeophysical measurements, in particular
63 resistivity loggings and electrical soundings. We assume the K distributions are local-stationary, i.e. the
64 mean and variance of log conductivity are convergent in each hydrofacies and in each local zone.
65 Therefore, we can compute the $\log_{10}(K)$ semivariogram in each hydrofacies and in each zone The Chaobai
66 alluvial fan in the northern Beijing Plain, China, was selected as study area to test the proposed integrated
67 approach.

68

69



70 2 Material and Methods

71 2.1 Study area

72 The study area belongs to the Chaobai River alluvial fan, in the northern Beijing Plain (northern latitude
 73 40°-40°30', eastern longitude 116°30'-117°), with an area of 1,150 km² (Fig. 1a). The Chaobai River is
 74 the second largest river flowing through the Beijing Plain from north to south. The ground elevation
 75 decreases southward with an average 2‰ slope. Quaternary sediments were mainly deposited by flooding
 76 events with turbulent flow and consist of porous strata containing groundwater. The aquifer system in the
 77 alluvial fan can be divided into three zones according to the lithological features (Fig. 1): an upper fan
 78 zone (or Zone 1) with coarse sediments (e.g., sandy-gravel aquifers), a middle upper fan zone (or Zone 2)
 79 where medium-coarse sediments (e.g., sandy-gravel to sandy-silt aquifers) were laid down , and a fine-
 80 sediment (e.g., sand and clay multiple aquifers) middle-lower fan zone (or Zone 3). Four hydrofacies,
 81 including sub-clay and clay (C), fine sand (FS), medium-coarse sand (MS), and gravel (G), were classified
 82 based on the interpretations of the cores and textural description of almost 700 boreholes (Zhu et al.,
 83 2015).

84 The study area is one of the most important regions for the supply of groundwater resource to Beijing.
 85 The Huairou emergency groundwater resource region (hereafter EGRR) with an area of 54 Km² is located
 86 in Zone 1. The total groundwater withdrawal amounted to 1.2×10⁸ m³ in 2003. Several well-fields
 87 belonging to the so-called "water supply factory" were drilled along the Chaobai River in Zone 1 and the
 88 upper Zone 2. Most of these well-fields were built in 1979 with a designed groundwater pumping volume
 89 of 1.6×10⁸ m³ per year. The average thickness of the exploited aquifer system is approximately 300 m.



90 The long-term over-exploration of the aquifer system has resulted in a serious drawdown of water levels,
91 which has reduced the exploitable groundwater resources and induced geological disasters, mainly land
92 subsidence, fault reactivation, and ground fissures (Cheng et al., 2015; Yang et al., 2015; Zhu et al., 2015).
93 In 2010, the annual groundwater withdrawal at the EGRR and the water factory decreased to 0.86×10^8
94 m^3 and $0.65 \times 10^8 \text{ m}^3$, respectively.

95 The largest cumulative land subsidence from June 2003 to January 2010 was quantified in approximately
96 340 mm by Zhu et al., (2013, 2015) in Tianzhu County to the south. The characterization of the
97 distribution and spatial variability of the hydraulic conductivity is vital for an optimal use of the limited
98 water resources in this area.

99 2.2 Methodological approach

100 Nowadays, a large set of hydraulic conductivity samples can be derived by integrating through appropriate
101 relations of various geological data, including hydrogeophysical measurements, borehole
102 lithostratigraphies, and hydrogeological information (total dissolved solid TDS and groundwater level).
103 These databases can be statistically processed to derive the spatial variation of $\log_{10}(K)$ for various facies,
104 including clay, fine sand, medium-coarse sand, and gravel.

105 In this paper, the statistical assessment is separately carried out for separated zones, building-up
106 experimental semivariograms that are fitted with exponential models. The optimal parameters of these
107 latter are estimated through a generalized output least squares (OLS) criterion. Then, the composite
108 semivariograms are computed using a hierarchical sedimentary architecture (Ritzi et al., 2004; Dai et al.,
109 2005) to obtain the K variance in each zone. Finally, the configuration of $\log_{10}(K)$ is simulated through a



multiple-zone sequential Gaussian algorithm with estimated statistic parameters reflecting the K spatial structures in the alluvial fan. Figure 2 shows the steps involved in the developed approach.

2.3 Data set

2.3.1 Geophysical data

Geophysical data include resistivity loggings and vertical electrical soundings. There are six well-electric logs continuously recording the formation resistivity versus depth. Five logs were collected in Zone 2 and one in Zone 3. Each well log has a lithological description, which helps to relate the resistivity values to the corresponding facies.

The average resistivity of G is the largest, with a value of $198 \Omega \text{ m}$, and that of C is the smallest with a value of $24 \Omega \text{ m}$. Figure 3 compares the outcome of logging data in term of resistivity versus depth and the corresponding stratigraphy, where the groundwater depth is 12 m. The log was acquired in the eastern part of Zone 2. The average resistivity from 32.4 m to 40.5 m depth, where the sediments are mainly G and MS, is $70.8 \Omega \text{ m}$. The resistivity curve shows two evident peaks from 97 m to 102 m and between 81 m and 84.5 m depth, where the MS is located.

The C resistivity is relatively low due to the good intrinsic electrical conductivity of this facies. For example from 16.5 m to 23.5 m depth, where C is the prevalent facies, a low resistivity equal to $27.2 \Omega \text{ m}$ is recorded. Since a hydrofacies with a smaller grain size has a greater total surface area, the resistivity difference can partially reflect the distributions of particle sizes and the hydrofacies composition.

Vertical electrical soundings (VES) using the Schlumberger electrode configuration were carried out by the Beijing Institute of Hydrogeology and Engineering Geology (BIHEG). A number of 113 detecting



positions were selected, with a maximum half current electrode space equal to 340 m and the potential electrode space ranging from 1 to 30 m. All the sounding data (1356 VES measurements) recorded the apparent resistivity of the porous medium. These data were inverted to real resistivity using the nonlinear Occam inversion method (Constable et al., 1987), with a low root mean square relative error of 2%.

2.3.2 Geological and hydrogeological data

Almost 700 borehole lithostratigraphies were collected in the study area. The sedimentary deposits show large heterogeneity from the upper to the lower fan zone. In Zone 1, the dominant facies is G with a volumetric proportion of 53%. The volumetric proportion of C is 16%. In Zone 2, the volumetric proportion of C increases to 40%, while that of G decreases sharply to 24%. In Zone 3, the proportion of G decreases further to 6% and that of C increases to 50% (Table 1). More detailed information is given in Zhu et al., (2016a). The lithological information in a buffer zone of 200 m around the VES locations has been used to represent the actual facies distribution in the surrounding of the geophysical acquisitions. A number of 35 hydrochemistry measurements with a depth from 20 m to 270 m were obtained throughout the area. The minimum, maximum and average TDS values are 423 mg/l at the depth of 180 m, 943 mg/l at the depth of 50 m, and 692 mg/l, respectively. Generally, the TDS is very low with the higher values measured in the south-western part of the study area. Because of the relatively small dataset and the observed low variability, in this paper the TDS variation in the vertical direction has been neglected. A TDS map was obtained by interpolating the available records using an Ordinary Kriging method with a spherical semivariogram model.



149 A large number of depth of water level measurements were also collected to map the thickness of the
150 unsaturated unit. The TDS and groundwater level at each VES and resistivity log location were derived
151 from the interpolated surfaces.

152 2.3.3 Hydraulic conductivity estimates from geophysical acquisitions

153 The hydraulic conductivity K was estimated using the Kozeny-Carman equation:

$$154 \quad K(x, y, z) = \frac{\delta g}{\mu} \times \frac{d_{(x,y,z)}^2}{180} \frac{\phi_{(x,y,z)}^3}{(1 - \phi_{(x,y,z)})^2} \quad (1)$$

155 which is widely accepted to derive the hydraulic conductivity from grain size and porosity (Soupios et
156 al., 2007; Utom et al., 2013; Khalil et al., 2013; Zhu et al., 2016). In Eq. (1), $d_{(x,y,z)}$ is the representative
157 grain diameter (mm) at location (x,y,z) , which was determined according to the lithology information, g
158 is gravity, μ the kinematic viscosity (kg/(m·s)), δ the fluid density, and $\phi_{(x,y,z)}$ the porosity. ϕ was
159 estimated using Archie's law (Eq. (2)), which relates the bulk resistivity of granular medium to porosity:

$$160 \quad \rho = \alpha \rho_w \phi^{-m} s_w^{-n} \quad (2)$$

161 where ρ is the saturated formation resistivity (Ω m), α the pore-geometry coefficient associated with the
162 medium ($0.5 \leq \alpha \leq 2.5$), m the cementation factor ($1.3 \leq m \leq 2.5$) (Massoud et al., 2010; Khalil and Santos
163 2013), s_w the water saturation, and n the saturation index. The pore fluid resistivity (Ω m) ρ_w is calculated
164 using the following experimental relation:

$$165 \quad \rho_w = \frac{5.6(\text{TDS})^b}{1 + \beta(t - 18)} \quad (3)$$

166 with TDS in (g/L), temperature t in ($^{\circ}\text{C}$), b and β being constant parameters (Wu et al., 2003). For the
167 most common electrolytes, $b = -0.95$ and $\beta = 0.025$.



The logarithmically transformed values of the estimated hydraulic conductivity ($\log_{10}(K)$) were used for the geostatistical analysis because of its normal distribution (Neuman, 1990). There are 102, 2077, and 1716 conductivity samples in Zone 1, Zone 2, and Zone 3, respectively. Considering that Archie's law can only be used for clay-free granular sediments, the K values of C were not estimated in this study. Based on available information, it has been reasonably assumed that clay fraction is negligible in G, MS, and FS facies. The statistics of $\log_{10}(K)$ for the three facies in three zones are listed in Table 2. The mean $\log_{10}(K)$ values decrease from Zone 1 to Zone 3, consistently with the sedimentary transport processes in the alluvial fan. In the upper region (Zone 1), high water flowing energy made the deposits consisted mainly of larger-grained particles and the coarse-grained sediments are dominant. In the southern part (Zone 3), the deposits change to relatively fine-grained particles. The mean $\log_{10}(K)$ of gravel is greater than 2.4 ($\log(\text{m/d})$) and that of fine sand is less than 0.2 ($\log(\text{m/d})$). The lithological information at the depth of the conductivity samples shows that volumetric proportions of FS and MS increase and that of G decreases from Zone 1 to Zone 3. The results are consistent with the statistic outputs deduced from 694 borehole data by Zhu et al., (2016a).

2.4 Statistical Methods

2.4.1 Semivariogram of hydraulic conductivity

Semivariogram describes the degree of spatial dependence of a spatial random field or stochastic process. It is a concise and unbiased characterization of the spatial structure of regionalized variables, which is important in Kriging interpolations and conditional simulations. The experimental semivariogram:

$$\hat{\gamma}_k(h_\varphi) = \frac{1}{2N(h)} \sum_{(o,p) \in N(h)} (Y(z_o) - Y(z_p))^2 \quad (4)$$



188 can be fitted by an exponential model (e.g., Dai et al., 2014b):

$$189 \quad r_k(h_\varphi) = \sigma^2(1 - e^{\frac{-3h}{\lambda}}) \quad (5)$$

190 where $\hat{r}_k(h_\varphi)$ and $r_k(h_\varphi)$ are the experimental and model semivariograms of log conductivity Y for the
 191 k^{th} facies at a lag distance h along the φ direction. In this paper we calculate the semivariograms in the
 192 vertical and dip directions. $N(h)$ is the number of pair measuring points z_o and z_p separated by a h lag
 193 distance, σ^2 is the variance, and λ the correlation range.

194 The variance and range were optimized using the least-squares criterion, which was solved by the
 195 modified Gauss-Newton-Levenberg-Marquardt method (Clifton and Neuman, 1982; Dai et al., 2012).

196 The sensitivity equation method was derived to compute the Jacobian matrix for iteratively solving the
 197 gradient-based optimization problem (Samper and Neuman 1986; Carrera and Neuman 1986; Dai and
 198 Samper, 2004; Samper et al., 2006; Yang et al., 2014; Zhu et al., 2016a). The two sensitivity coefficients

199 $\frac{\partial r_k}{\partial \sigma^2}$ and $\frac{\partial r_k}{\partial \lambda}$ are the partial derivatives of the semivariogram with respect to variance and range:

$$200 \quad \frac{\partial r_k}{\partial \sigma^2} = 1 - e^{\frac{-3h}{\lambda}} \quad (6)$$

$$201 \quad \frac{\partial r_k}{\partial \lambda} = -\sigma^2 \cdot 3h \cdot e^{\frac{-3h}{\lambda}} \cdot \lambda^{-2} \quad (7)$$

202

203 2.4.2 Composite semivariogram of log conductivity

204 Once the facies semivariograms were obtained in each zone, the composite semivariogram $\gamma(h)$ could be
 205 calculated through the following equation (e.g., Ritzi et al., 2004):



$$\gamma(h_\varphi) = \sum_{k=1}^M \sum_{i=1}^M r_{ki}(h_\varphi) p_k t_{ki}(h_\varphi) \quad (8)$$

where p_k and $t_{ki}(h_\varphi)$ are the volumetric proportion of facies k and the transition probability from facies k to facies i in the φ direction with a h lag distance, respectively. Equation 8 delineates the composite semivariogram with respect to the individual facies semivariogram and transition probability. The general shape function and range of the composite semivariogram can be obtained from individual facies mean length and volumetric proportion with the methods described in Dai et al., (2005).

The transition probability $t_{ki}(h_\varphi)$ has an analytical solution as derived by Dai et al., (2007):

$$t_{ki}(h_\varphi) = p_k + (\delta_{ki} - p_k) \cdot \exp\left(\frac{h_\varphi}{\lambda_\varphi}\right) \quad (9)$$

where δ_{ki} is the Kronecker delta and λ_φ is the integral scale in the direction of φ . A geostatistical modeling tool GEOST (Dai et al., 2014b) modified from the Geostatistical Software Library (Deutsch and Journel, 1992) and TPROGS (Carle and Fogg, 1997) was employed to compute the sample transition probabilities in each zone. The parameters p_k and λ_φ were optimally estimated through a modified Gauss-Newton-Levenberg-Marquardt method. More details are provided by Zhu et al., (2016a). The composite semivariograms for different zones can help us to understand the heterogeneity variations from the upper to lower part of the alluvial fan, as well as the stationary property (local versus regional) of the facies and hydraulic conductivity distributions.

2.4.3 Sequential Gaussian simulation

The Sequential Gaussian simulation (SGSIM) is a widely used stochastic simulation method to create numerical model of continuous variables based on the Gaussian probability density function. The process



is assumed to be a stationary and ergodic random process (Deutsch and Journel, 1992; Dimitrakopoulos and Luo, 2004). This method can preserve the variance and correlation range observed in spatial samples. SGSIM provides a standardized normal continuous distribution of the simulated variable.

With the assumption that the log conductivity distributions are stationary within each zone, we used SGSIM simulator implemented into GEOST to model the $\log_{10}(K)$ continuous configuration under a multiple-zone framework. The conductivity of the FS, MS, and G facies in each zone was simulated sequentially using the structure characteristics of the semivariograms.

Finally, the three-dimensional conductivity configuration was derived by combining the stochastic simulated facies (Zhu et al., 2016a) with the SGSIM conductivity distribution and the mean $\log_{10}(K)$ of the various facies in each zone (Table 2). In detail, since each cell is characterized by specific facies and zone indices, its conductivity was assigned using the corresponding (in relation to the facies and the zone) 3D SGSIM outcome in that position. Since sub-clay and clay are generally characterized by a low hydraulic conductivity value, a uniform K value equal to 0.0001 m/d was set to all the C cells.

3 Results and Discussion

3.1 Variation of $\log_{10}(K)$ for the various facies

The optimized vertical correlation range and variance of the log conductivity semivariogram (Eq. 5) are listed in Table 3, along with their 95% confidence intervals. The fitting between the experimental and the model semivariograms is the best in Zone 2 because of the abundant samples, while the fitting in Zone 1 is the worst (Fig. 4). The fitting result of the semivariogram for the G facies is the worst in Zone 1. Two are the reasons: the first is the high variance of gravel in this zone; the other is the limited number of



245 samples (102 samples), which makes quite small the pair numbers within each lag spacing. Hence, the
 246 computed semivariogram is highly uncertainty.

247 The variance of FS, MS, and G in the vertical direction decreases from Zone 1 to Zone 3. In the upper
 248 alluvial fan, sediments were deposited under multiple water flowing events and with bad sorting. The
 249 deposits consist of wide ranges of sediment categories and grain sizes. The variance of G is larger than
 250 1.5, which reflects the high heterogeneity in coarse deposits. The variances of FS and MS are smaller
 251 with values equal to 0.23 and 0.32, respectively. In Zone 3, these values decrease to 0.05 and 0.13,
 252 respectively, with that of G sharply decreasing to 0.62. In the middle-lower fan zone, the conductivity
 253 variation within each facies reduces gradually because the ground surface slope becomes smaller or flat,
 254 the sediment transport energy decreases, and the deposits within the three facies have a good sorting.

255 Note that the ranges are correlated with the facies structure parameters such as the indicator correlation
 256 scale, mean thickness (or length), and volumetric proportion (Dai et al., 2004b; 2007). The estimated
 257 correlation ranges of FS, MS and G along the vertical direction in Zone 1 do not show big difference with
 258 values equal to 6.0 m, 8.0 m and 6.5 m, respectively. In Zone 2, the ranges of three facies change a lot.
 259 The range of G is almost five and two times that of FS and MS, respectively. Conversely, the range
 260 difference among the facies decreases sharply in Zone 3. The range of G is alike to that of FS with a value
 261 of about 6.0 m, similarly as in Zone 1, and twice as much that of MF. The variation of the structure
 262 parameters of three facies causes the large changes of the correlation ranges from Zone 1 to Zone 3.

263 Due to the small number of conductivity samples in Zone 1, the variance of $\log_{10}(K)$ along the dip
 264 direction is calculated only in Zone 2 and Zone 3 (Table 4). The variance of G, MS and FS in Zone 2 is



265 higher than that in Zone 3, as observed along vertical direction. In Zone 2, the variance of FS, MS and G
 266 in the dip direction is gently larger than that along the vertical direction. This occurrence possibly reflects
 267 multiple flooding events that caused particles deposited along the dip direction more heterogeneously
 268 than in the vertical direction during the formation process of Zone 2. Conversely, the variance associated
 269 FS, MS and G is smaller along the dip direction than the vertical one in Zone 3.

270 3.2 Composited semivariogram of $\log_{10}(K)$

271 The composite semivariogram in the vertical direction at each zone is calculated by Eq. (8), using the
 272 volume proportion (Table 1) and transition probability (Eq. (9)) with the same values of the lag distance
 273 used to compute the facies semivariograms. The values of the optimized variance are 0.68, 0.11, and 0.03
 274 in Zone 1, Zone 2, and Zone 3, respectively. The high flow energy and the large number of flooding
 275 events contributing to sediment deposition are the main causes of the high heterogeneity (largest variance)
 276 of the deposits in the upper part of the alluvial fan. The changes of variance between the three zones
 277 support the utilization of the local-stationary assumption and simulation of multiple-zone based
 278 conductivity distributions for the Chaobai alluvial fan.

279 3.3 Configuration of $\log_{10}(K)$

280 The configuration of $\log_{10}(K)$ in three dimensions is showed in Fig.7. The distribution of conductivity is
 281 generally consistent with that of the facies. The conductivity of large grain-size sediments is generally
 282 larger, thus on the average K is much larger in the upper zone than in the lower part of the alluvial fan.
 283 The regions with high conductivity (red color in Fig. 7) in Zone 1 are more continuous than that in other
 284 parts. The adjacent cells with the smallest conductivity (blue color in Fig. 7) are obviously located mainly



285 in Zone 3. The mean conductivity is smaller in the southern part of the study area, where the piezometric
286 drawdowns in the multi-layer aquifer system were larger and the surface subsidence more serious (Zhu
287 et al., 2013, 2015).

288 Based on the three dimensional K configuration, the average value of K in the depth range from 0 m to
289 300 m amounts to 194 m/d, 25 m/d and 4 m/d in Zone 1, Zone 2, and Zone 3, respectively. These values
290 are comparable with those provided by the Beijing Institute of Hydrogeology and Engineering Geology
291 (2007) based on a number of pumping tests carried out over several years in the study area. In this BIHEG
292 report the average value of K is >300 m/d in Zone 1, between 30 and 100 m/d in Zone 2, and <30 m/d
293 in Zone 3 (Fig. 1b). The fact that our average K values is gently smaller than these latter is likely due to
294 the fact that the outcome of pumping tests are generally more representative of coarser sediments.
295 Conversely, those estimated from the stochastic framework represent more properly the heterogeneous
296 distributions of the hydraulic conductivity (Zhu et al., 2016b).

297 Investigating the stochastic results along the vertical direction, it is interesting to notice that the average
298 K in deep units of Zone 1 and Zone 2 is smaller than that in the shallow strata. For example, in Zone 1
299 the average K for the cells from 0 m to 100 m deep is 295 m/d, which is three times as much the value for
300 the depth range between 200 m and 300 m. Conversely, no significant variation of K versus depth is
301 observed in Zone 3, with only a small decrease of the average K from the deeper to the shallower units.

302 4 Conclusions

303 This paper proposes a geostatistical method under a multiple zone framework, properly supported by a
304 large number of geophysical investigations, to detect the distribution and the related variance of the



305 hydraulic conductivity in three-dimensional domains. In particular, the optimized statistical parameters
 306 (e.g., log conductivity variance and correlation range) of semivariograms are estimated using the modified
 307 Gauss-Newton-Levenberg-Marquardt method. The Chaobai alluvial fan is used as a case study area.
 308 Multiple data including downhole resistivity logging data, vertical electric soundings, well-bore
 309 lithostratigraphies, TDS measurements, and depths to the water table are integrated to derive a dataset of
 310 conductivity values in a three-dimensional setting. Log conductivity semivariograms fitted with
 311 exponential functions are built-up for three facies, including fine sand, medium-coarse sand and gravel,
 312 in each of the three zones into which the Chaobai fan is divided to guarantee local stationarity of the
 313 statistical process. The composite semivariogram of the three facies has been derived for the two zones
 314 where a sufficiently large number of samples are available. The $\log_{10}(K)$ configuration is simulated using
 315 the sequential Gaussian simulation model based on statistic parameters of $\log_{10}(K)$ and the structure
 316 suggested by a 3D hydrofacies simulation.

317 For the specific test case, the variance along the vertical direction of fine sand, medium-coarse sand, and
 318 gravel decreases from the upper part of the alluvial fan, where the values amount to 0.23, 0.32, and 1.60,
 319 to the lower portion of the Chaobai plan with values of 0.05, 0.126, and 0.62, respectively. This behavior
 320 reflects the higher transport energy in the upper alluvial fan that causes a bad sediment sorting. In the
 321 middle alluvial fan, the transport energy decreases and the sediments tend to be relatively good-sorted.
 322 The variance of the gravel is larger than that of other lithologies. The different flow energy significantly
 323 affected the coarse sediments in the vertical direction. Along the dip direction, the variance of three facies
 324 (gravel, medium-coarse sand and fine sand) in the middle fan is larger than that in the lower fan. The



325 composite variance of $\log_{10}(K)$ in the vertical direction shows that the large heterogeneity in the upper
326 fan (with a value of 0.68) decreases in the lower zone.

327 The distribution of hydraulic conductivity is consistent with that of the facies. Hydraulic conductivity is
328 much larger in the upper zone than that in the lower part of the alluvial fan. This result provides valuable
329 insights for understanding the spatial variations of hydraulic conductivity and setting-up groundwater
330 flow, transport, and land subsidence models in alluvial fans.

331 Concluding, it is worth highlighting that we depicted an original method to detect the variance and
332 configuration of conductivity by fusing multiple-source data in three-dimensional domains. The proposed
333 approach can be easily used to statistically characterize the hydraulic conductivity of the various alluvial
334 fans that worldwide are strongly developed to provide high-quality water resources. We are aware of
335 some restrictions in the dataset available at the date for the Chaobai alluvial fan, for example the assumed
336 uniform distribution of TDS versus depth and the relatively small number of the conductivity samples in
337 the upper fan zone. Nonetheless, the proposed methodology will be re-applied in the near future as soon
338 as new information will become available, thus allowing to improve the estimation accuracy of spatial
339 statistics parameters and the configuration of hydraulic conductivity in this Quaternary system so
340 important for the Beijing water supply.

341 **Data availability**

342 The geophysical measurements, borehole lithostratigraphies, and hydrogeological information in the
343 north part of Beijing Plain can be partly accessible by contacting Beijing Institute of Hydrogeology and
344 Engineering Geology.



345 **Author contribution**

346 Lin Zhu, Huili Gong and Zhenxue Dai derived the method of spatial variance and 3D configuration of
347 conductivity, performed data analysis and wrote the draft manuscript. Gaoxuan Guo collected the
348 geological and geophysical data, discussed the results. Pietro Teatini discussed the results, reviewed and
349 revised the manuscript.

350 **Competing interests**

351 The authors declare that they have no conflict of interest.

352 **Acknowledgements**

353 This work was supported by the National Natural Science Foundation (No.41201420, 41130744) and
354 Beijing Nova Program (No.Z111106054511097). Pietro Teatini was partially supported by the University
355 of Padova, Italy, within the 2016 International Cooperation Program.

356 **References**

- 357 Anderson, M.P.: Introducing groundwater physics, Phys. Today, 42–47, 2007
- 358 Beijing Institute of Hydrogeology and Engineering Geology: Groundwater flow model and the potential
359 groundwater resources in Beijing Plain, Internal Report, 60-64., 2007 (In Chinese)
- 360 Bevington, J., Piragnolo, D., Teatini, P., Vellidis, G., and Morari, F.: On the spatial variability of soil
361 hydraulic properties in a Holocene coastal farmland, Geoderma, 262: 294-305,
362 doi:10.1016/j.geoderma.2015.08.025, 2016.
- 363 Carle, S.F., and Fogg, G.E.: Modeling spatial variability with one and multimensional continuous-lag
364 Markov chain, Math. Geol., 29: 891-918, doi: 10.1023/a:1022303706942, 1997.



- 365 Carrera, J., and Neuman, S.P.: Estimation of aquifer parameters under steady state and transient condition:
 366 2. Uniqueness, stability, and solution algorithms, *Water Resour. Res.*, 22, 211 – 227, doi:
 367 10.1029/wr022i002p00211, 1986.
- 368 Cheng, G., Wang, H., Luo, Y., and Guo, H.: Study of the deformation mechanism of the Gaoliying ground
 369 fissure: Prevention and Mitigation of Natural and Anthropogenic Hazards due to Land Subsidence - Proc.
 370 IX Int. Symp. on Land Subsidence, K. Daito et al. eds., Proc. IAHS, UK, 231-234, 2015.
- 371 Clifton, P.M., and Neuman, S.P.: Effects of kriging and inverse modeling on conditional simulation of
 372 the Avra Valley aquifer in southern Arizona, *Water Resour. Res.*, 18, 1215-1234, doi:
 373 10.1029/wr018i004p01215, 1982.
- 374 Constable, S.C., Parker, R.L., and Constable, C.G.: Occam's inversion: A practical algorithm for
 375 generating smooth models from electromagnetic sounding data, *Geophysics*, 52, 289-300, 1987.
- 376 Dai, Z., and Samper, J.: Inverse problem of multicomponent reactive chemical transport in porous media:
 377 Formulation and applications, *Water Resour. Res.*, 40, W07407, doi: 10.1029/2004wr003248, 2004.
- 378 Dai, Z., Ritzi, R., and Dominic, D.: Estimating parameters for hierarchical permeability correlation
 379 models. *Aquifer Characterization*, Bridge, J.S. and Hyndman, D.W. SEPM Society for Sedimentary
 380 Geology, USA, 41-54, doi: 10.2110/pec.04.80.0041, 2004a.
- 381 Dai, Z., Ritzi, R., Huang, C., Dominic, D., and Rubin, Y.: Transport in heterogeneous sediments with
 382 multimodal conductivity and hierarchical organization across scales, *J. of Hydrology*, 294, 68-86, doi:
 383 10.1007/s00477-014-0922-3, 2004b.
- 384 Dai Z., Ritzi, R., and Dominic, D.: Improving permeability semivariograms with transition probability
 385 models of hierarchical sedimentary architecture derived from outcrop analog studies. *Water Resour. Res.*,
 386 14 W07032, doi: 10.1029/2004wr003515, 2005.
- 387 Dai, Z., Wolfsberg, A., Lu, Z., and Ritzi, R.: Representing aquifer architecture in macrodispersivity
 388 models with an analytical solution of the transition probability matrix. *Geophys. Res. Lett.*, 34, L20406,
 389 doi: 10.1029/2007GL031608, 2007.



- 390 Dai, Z., Wolfsberg, A., Reimus, P., Deng, H., Kwicklis, E., Ding, M., Ware, D., and Ye, M.: Identification
391 of sorption processes and parameters for radionuclide transport in fractured rock, *J. Hydrol.*, 414-415,
392 220-230, doi: 10.1016/j.jhydrol.2011.10.035, 2012.
- 393 Dai, Z., Viswanathan, H., Fessenden-Rahn, J., Middleton, R., Pan, F., Jia, W., Lee, S., McPherson, B.,
394 Ampomah, W., and Grigg, R.: Uncertainty quantification for CO₂ sequestration and enhanced oil recovery,
395 *Energy Procedia*, 63, 7685–7693, 2014a.
- 396 Dai, Z., Middleton, R., Viswanathan, H., Fessenden-Rahn, J., Bauman, J., Pawar, R., Lee, S., and
397 McPherson, B.: An integrated framework for optimizing CO₂ sequestration and enhanced oil recovery.
398 *Environ. Sci. Technol. Lett.*, 1, 49-54, doi: 10.1021/ez4001033, 2014b.
- 399 Deutsch, C.V., and Journel, A.G. *GSLIB: Geostatistical software library*, Oxford Univ. Press. New York,
400 340, 1992.
- 401 Dimitrakopoulos, R., and Luo, X.: Generalized sequential Gaussian simulation on group size v and
402 screen-effect approximations of large field simulations. *Math. Geol.*, 36, 567-590, doi:
403 10.1023/b:matg.0000037737.11615.df, 2004.
- 404 Eggleston, J., and Rojstaczer, S.: Identification of large-scale hydraulic conductivity trends and the
405 influence of trends on contaminant transport. *Water Resour. Res.*, 34, 2155-2186, doi:
406 10.1029/98wr01475, 1998.
- 407 Harp, D., Dai, Z., Wolfsberg, A., and Vrugt, J.: Aquifer structure identification using stochastic inversion,
408 *Geophys. Res. Lett.*, 35, L08404, doi: 10.1029/2008gl033585, 2008.
- 409 Hinnell, A.C., Ferre, T.P.A., Vrugt, J., Huisman, J.A., Moysey, S., Rings, J., and Kowalsky, M.B.:
410 Improved extraction of hydrologic information from geophysical data through coupled hydrogeophysical
411 inversion. *Water Resour. Res.*, 46, doi: 10.1029/2008wr007060, 2010.
- 412 Hubbard, S.S., Chen, J.S., Peterson, J., Majer, E.L., Williams, K.H., Swift, D.J., Mailloux, B., and Rubin,
413 Y.: Hydrogeological characterization of the South Oyster Bacterial Transport site using geophysical data,
414 *Water Resour. Res.*, 37, 2431-2456, doi: 10.1029/2001wr000279, 2001.



- Irving, J., and Singha, K.: Stochastic inversion of tracer test and electrical geophysical data to estimate hydraulic conductivities, *Water Resour. Res.*, 46, W11514, doi: 10.1029/2009WR008340, 2010.
- Khalil, M.A., and Santos, F.A.M.: Hydraulic conductivity estimation from resistivity logs: a case study in Nubian sandstone aquifer. *Arab. J. Geosci.*, 6, 205-212. doi: 10.1007/s12517-011-0343-2, 2013.
- Massoud, U., Santos, F.A.M., Khalil, M. A., Taha, A., and Abbas, A. M.: Estimation of aquifer hydraulic parameters from surface geophysical measurements: a case study of the Upper Cretaceous aquifer, central Sinai, Egypt, *Hydrogeol. J.*, 18, 699-710, doi: 10.1007/s10040-009-0551-y, 2010.
- Morin, R.H.: Negative correlation between porosity and hydraulic conductivity in sand-and-gravel aquifers at Cape Cod, Massachusetts, USA, *J. Hydrol.*, 316, 43-52, doi:10.1016/j.jhydrol.2005.04.013, 2006.
- Neuman, S.P.: Universal scaling of hydraulic conductivities and dispersivities in geologic media, *Water Resour. Res.*, 26, 1749-1758, 1990.
- Niwas, S., and Singhal, D.C.: Aquifer transmissivity of porous media from resistivity data, *J. Hydrol.*, 82, 143-153, doi: 10.1016/0022-1694(85)90050-2, 1985.
- Niwas, S., Tezkan, B., and Israil, M.: Aquifer hydraulic conductivity estimation from surface geoelectrical measurements for Krauthausen test site, Germany, *Hydrogeol. J.*, 19, 307-315, doi: 10.1007/s10040-010-0689-7, 2011.
- Niwas, S., and Celik, M.: Equation estimation of porosity and hydraulic conductivity of Ruhrtal aquifer in Germany using near surface geophysics. *J. Appl. Geophys.*, 84, 77-85, doi: 10.1016/j.jappgeo.2012.06.001, 2012.
- Proce, C., Ritzi, R. W., Dominic, D., and Dai, Z.: Modeling multiscale heterogeneity and aquifer interconnectivity, *Ground Water*, 42, 658-670, 2004.
- Ritzi, R., Dominic, D.F., Slesers, A.J., and Greer, C.B.: Comparing statistical models of physical heterogeneity in buried-valley aquifers. *Water Resour. Res.*, 36, 3179-3192, doi: 10.1029/2000wr900143, 2000.



- 440 Ritzi R., Dai, Z., and Dominic, D.: Spatial correlation of permeability in cross-stratified sediment with
 441 hierarchical architecture. *Water Resour. Res.*, 40, W03513, doi: 10.1029/2003wr002420, 2004.
- 442 Samper, F.J., and Neuman, S.P.: Adjoint state equations for advective-dispersive transport: Proceeding
 443 of the 6th International Conference in Finite Elements in Water Resource, 423-437, New York, doi:
 444 10.1007/978-3-662-11744-6_31, 1986.
- 445 Samper, J., Dai, Z., Molinero, J., García-Gutiérrez, M., Missana, T., and Mingarro, M.: Inverse modeling
 446 of tracer experiments in FEBEX compacted Ca-bentonite. *Physics and Chemistry of the Earth*, 31, 640-
 447 648, 2006.
- 448 Sikandar, P., Bakhsh, A., Arshad, M., and Rana, T.: The use of vertical electrical sounding resistivity
 449 method for the location of low salinity groundwater for irrigation in Chaj and Rachna Doabs, *Environ.*
 450 *Earth Sci.*, 60, 1113-1129, doi: 10.1007/s12665-009-0255-6, 2010.
- 451 Soltanian, M.R., Ritzi, R.W., Huang, C.C., and Dai, Z.: Relating reactive solute transport to hierarchical
 452 and multiscale sedimentary architecture in a Lagrangian-based transport model: 2: Particle displacement
 453 variance. *Water Resour. Res.*, 51, 1601-1618, doi: 10.1002/2014wr016354, 2015.
- 454 Soupios, P.M., Kouli, M., Vallianatos, F., Vafidis, A., and Stavroulakis, G.: Estimation of aquifer
 455 hydraulic parameters from surficial geophysical methods: A case study of Keritis Basin in Chania (Crete-
 456 Greece), *J. Hydrol.*, 338, 122-131, doi: 10.1016/j.jhydrol.2007.02.028, 2007.
- 457 Utom, A.U., Odoh, B.I., Egboka, B.C.E., Egboka, N.E., and Okeke, H.C.: Estimation of subsurface
 458 hydrological parameters around Akwuke, Enugu, Nigeria using surface resistivity measurements. *J.*
 459 *Geophys. Eng.*, 10, 025016, doi: 10.1088/1742-2132/10/2/025016, 2013.
- 460 Weissmann, G.S., and Fogg, G.E.: Multi-scale alluvial fan heterogeneity modeled with transition
 461 probability geostatistics in a sequence stratigraphic framework. *J. Hydrol.*, 226, 48–65, doi:
 462 10.1016/S0022-1694(99)00160-2, 1999.



- 463 Wu, Y., Guo, J., and Qiang, J.: Assessing the total dissolved solid in groundwater on basis of resistivity.
 464 Conference on Groundwater Survey and Monitoring Technology, Baoding Hebei, China, 2003. (In
 465 Chinese)
- 466 Yang, C., Dai, Z., Romanak, K., Hovorka, S., and Trevino, R.: Inverse Modeling of Water-Rock-CO₂
 467 Batch Experiments: Implications for Potential Impacts on Groundwater Resources at Carbon
 468 Sequestration Sites, Environ. Sci. Technol., 48, 2798–2806, doi: 10.1021/es4041368, 2014.
- 469 Yang, Y., Luo, Y., Liu, M., Wang, R., and Wang, H.: Research of features related to land subsidence and
 470 ground fissure disasters in the Beijing Plain: Prevention and Mitigation of Natural and Anthropogenic
 471 Hazards due to Land Subsidence - Proc. IX Int. Symp. on Land Subsidence, K. Daito et al. eds., Proc.
 472 IAHS,UK, 372, 239-242, 2015.
- 473 Yeh, T.C., Liu, S., Glass, R.J., Baker, K., Brainard, J.R., Alumbaugh, D., and LaBrecque, D.: A
 474 geostatistically based inverse model for electrical resistivity surveys and its applications to vadose zone
 475 hydrology. Water Resour. Res., 38, 1278, doi: 10.1029/2001wr001204, 2002.
- 476 Zappa, G., Bersezio, R., Felletti, F., and Giudici, M.: Modeling heterogeneity of gravel-sand, braided
 477 stream, alluvial aquifers at the facies scale. J. Hydrol., 325,134-153, doi :10.1016/j.jhydrol.2005.10.016,
 478 2006.
- 479 Zhu, L., Gong, H., Li, X., Li, Y., Su, X., and Guo, G.: Comprehensive analysis and artificial intelligent
 480 simulation of land subsidence of Beijing, China. Chin. Geogra. Sci., 23, 237–248, doi: 10.1007/s11769-
 481 013-0589-6, 2013.
- 482 Zhu, L., Gong, H., Li, X., Wang, R., Chen, B., Dai, Z., and Teatini, P.: Land subsidence due to
 483 groundwater withdrawal in the northern Beijing plain, China, Eng. Geol., 193, 243-255, doi:
 484 10.1016/j.enggeo.2015.04.020, 2015.
- 485 Zhu, L., Dai, Z., Gong, H., Gable, C., and Teatini, P.: Statistic inversion of multi-zone transition
 486 probability models for aquifer characterization in alluvial fans. *Stoch. Environ. Res. Risk Assess.*, 30,
 487 1005-1016, doi: 10.1007/s00477-015-1089-2, 2016a.



488 Zhu, L., Gong, H., Chen, Y., Li, X., Chang, X., and Cui, Y.: Improved estimation of hydraulic
489 conductivity by combining stochastically simulated hydrofacies with geophysical data. Sci. Rep., 6,
490 22224, doi: 10.1038/srep22224, 2016b.



Table 1 Values of the volumetric proportion for the various facies in three zones

Zone	Sub-clay and clay	Fine sand	Medium-coarse sand	Gravel
Zone 1	0.166	0.234	0.067	0.533
Zone 2	0.409	0.286	0.065	0.240
Zone3	0.503	0.328	0.106	0.063

Table 2 Statistical data of logarithm hydraulic conductivity ($\log_{10}(\text{m/d})$) in the three zones of the Chaobai alluvial fan

Zone	Parameter	Fine sand	Medium-coarse sand	Gravel
Zone 1	Mean	1.07	1.82	2.92
	Minimum	-0.94	1.22	2.26
	Maximum	1.65	2.45	3.66
	Proportion	0.36	0.12	0.32
Zone 2	Mean	0.42	1.17	2.65
	Minimum	-2.22	-0.23	0.95
	Maximum	1.22	2.07	3.38
	Proportion	0.23	0.14	0.31
Zone 3	Mean	0.17	0.81	2.48
	Minimum	-2.64	-0.78	0.34
	Maximum	0.72	1.43	3.21
	Proportion	0.35	0.17	0.12



Table 3 Optimized parameters in the fitting exponential function of $\log_{10}(K)$ semivariogram in vertical direction for the various facies and zones

Zone	Parameter	Fine sand		Medium-coarse sand		Gravel	
		Estimated value	Confidence Interval (95%)	Estimated value	Confidence Interval (95%)	Estimated value	Confidence Interval (95%)
Zone 1	Variance	0.23	(0.19, 0.28)	0.32	(0.29, 0.34)	1.60	(1.41, 1.81)
	Range (m)	6.01	(2.01, 20.52)	8.01	(1.53, 14.67)	6.50	(6.5, 12.84)
Zone 2	Variance	0.069	(0.067, 0.070)	0.14	(0.13, 0.15)	1.22	(1.19, 1.24)
	Range (m)	3.13	(1.83, 4.42)	8.27	(3.61, 12.93)	15.0	(12.33, 17.67)
Zone3	Variance	0.05	(0.047, 0.053)	0.126	(0.118, 0.135)	0.62	(0.54, 0.7)
	Range (m)	6.52	(2.19, 10.85)	2.72	(0.20, 6.55)	5.98	(0.20, 15.63)

Table 4 Variance of $\log_{10}(K)$ of different facies along the dip direction in Zone 2 and Zone 3

Zone		Fine sand	Medium-coarse sand	Gravel
Zone 2	Estimated value	0.10	0.15	1.38
	Confidence Interval (95%)	(0.059, 0.141)	(0.071, 0.228)	(1.14, 1.62)
Zone 3	Estimated value	0.045	0.068	0.48
	Confidence Interval (95%)	(0.030, 0.0607)	(0.043, 0.093)	(0.22, 0.73)



516 **Figure captions**

517 Figure 1 Chaobai alluvial fan in the north of Beijing Plain. (a) Location of the study area and distribution
 518 of the field data. (b) Map of the hydraulic conductivity issued by Beijing Institute of Hydrogeology and
 519 Engineering Geology (2007). The location of the study area is shown in the inset.

520 Figure 2 Flowchart of the geostatistical methodology

521 Figure 3 Typical depth behaviour of resistivity and corresponding stratigraphy in the eastern part of Zone
 522 2

523 Figure 4 Experimental (circle symbol) and model (solid line) semivariogram along the vertical direction
 524 for the various hydrofacies in the three zones. Notice that the range in the y-axis differs for sands and
 525 gravel lithologies in Zone 2 and Zone 3.

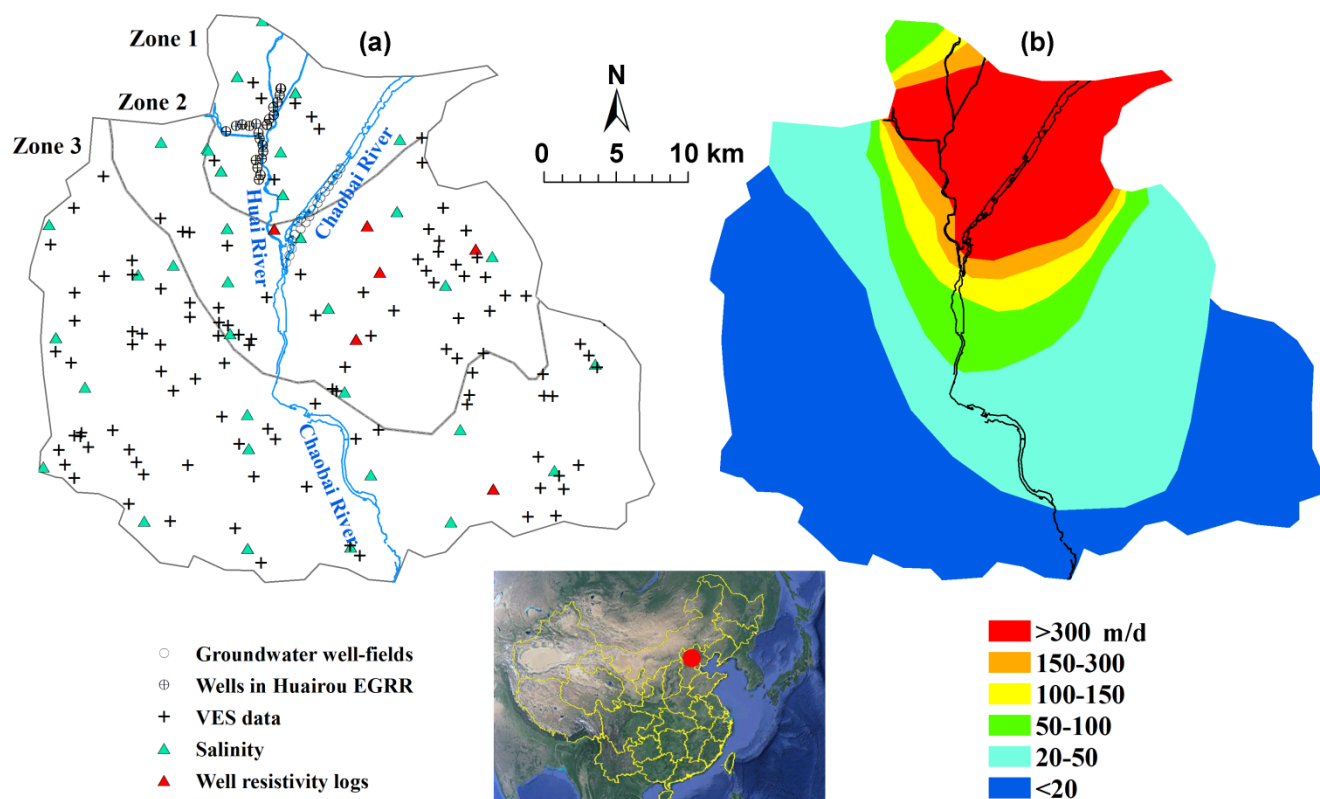
526 Figure 5 Experimental (circle symbol) and model (solid line) semivariogram along the dip direction for
 527 the various hydrofacies in Zone 2 and Zone 3.

528 Figure 6 Experimental (circle symbol) and model (solid line) composited semivariogram along the
 529 vertical direction for the three zones.

530 Figure 7 Distribution of hydrofacies (after Zhu et al., 2015a) and $\log_{10}(K)$ in the three-dimensional domain
 531 representing the Chaobai alluvial fan: (a) axonometric projection of the three-dimensional system and (b)
 532 vertical sections along the A-A', B-B', C-C' and D-D' alignments. The vertical exaggeration is 25. The
 533 selected cell size is 300 m in north-south and east-west directions and 5 m in vertical direction, with a
 534 total number of 747, 540 cells. The thickness of the simulated domain is 300 m.



535 **Figure 1**



536



Figure 2

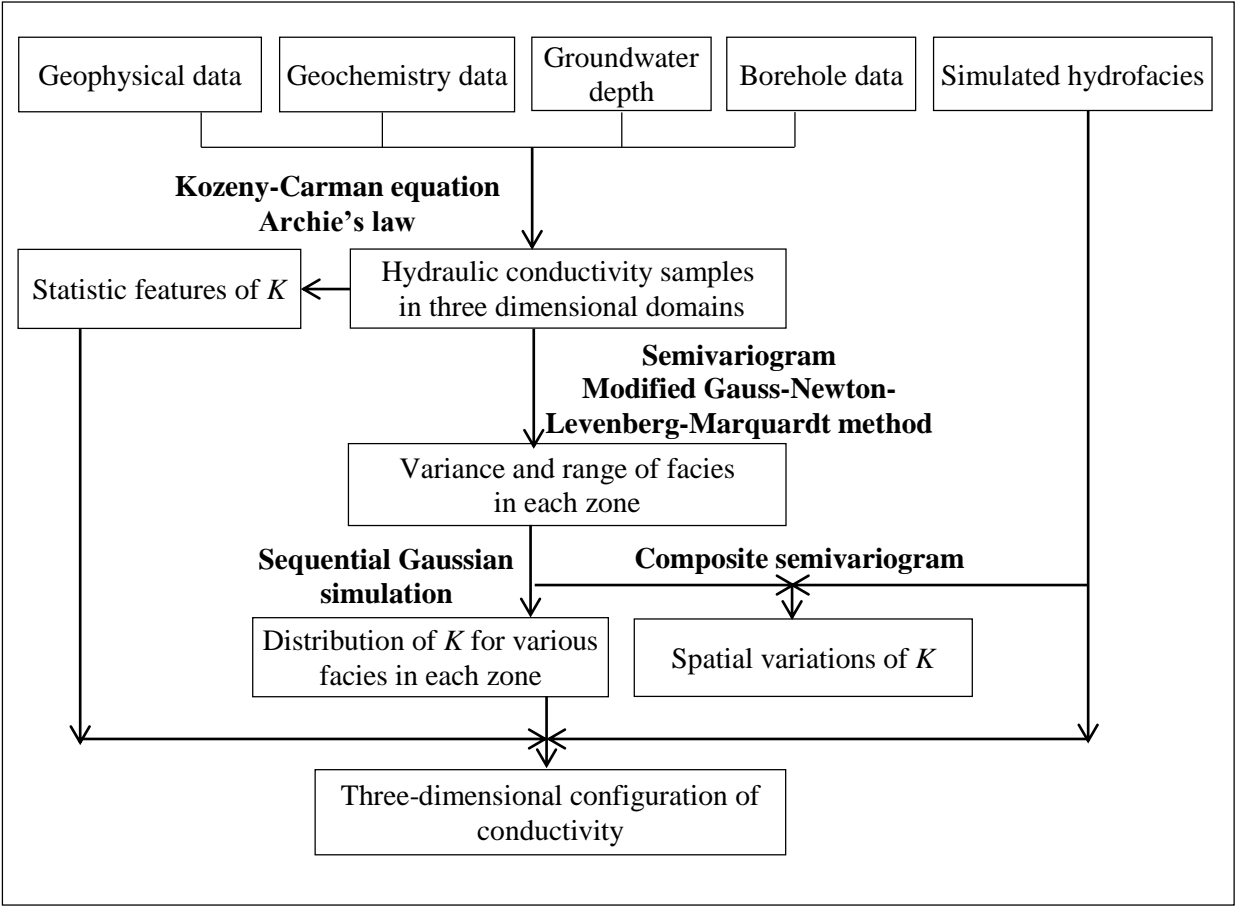




Figure3

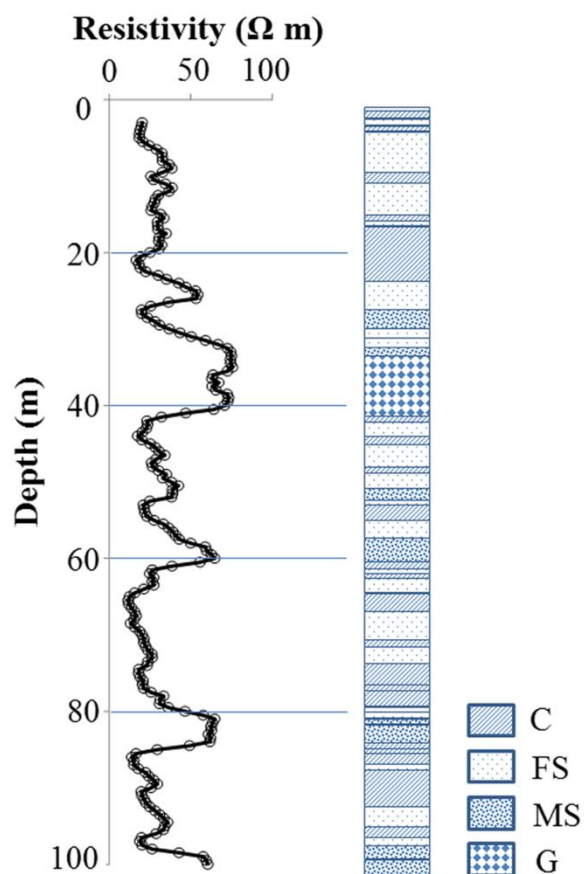
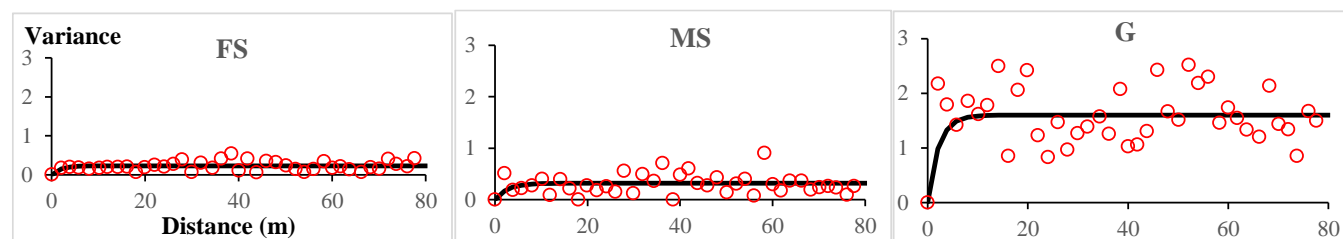
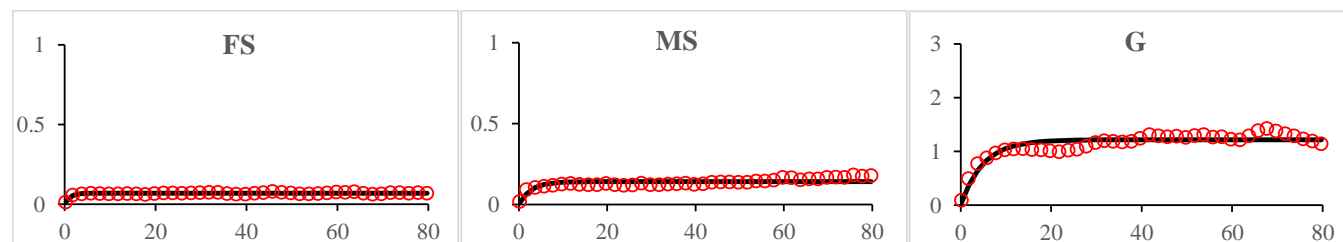




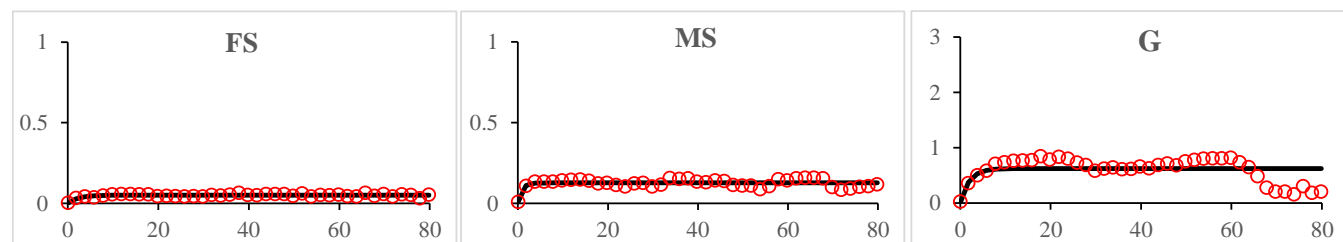
Figure 4



Zone 1



Zone 2



Zone 3



Figure 5

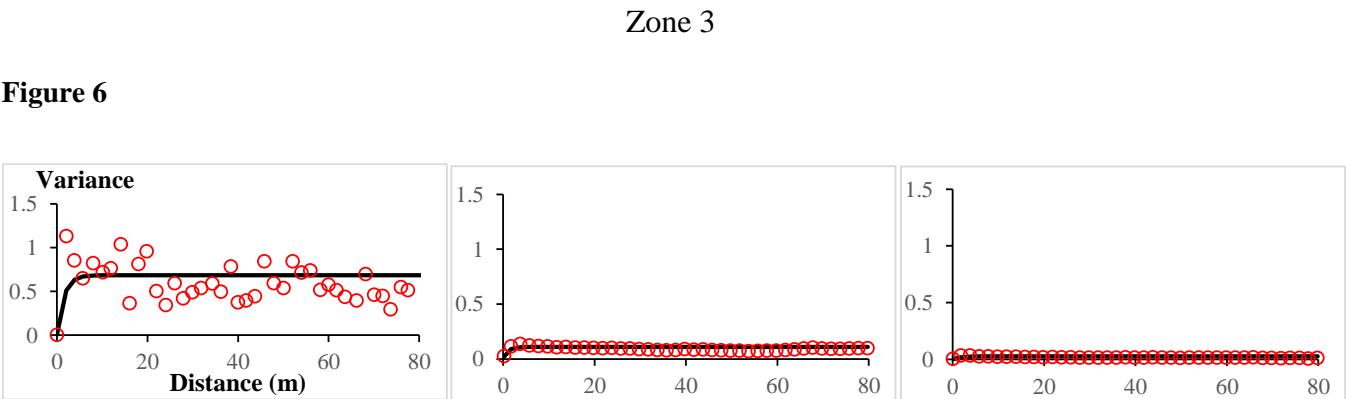
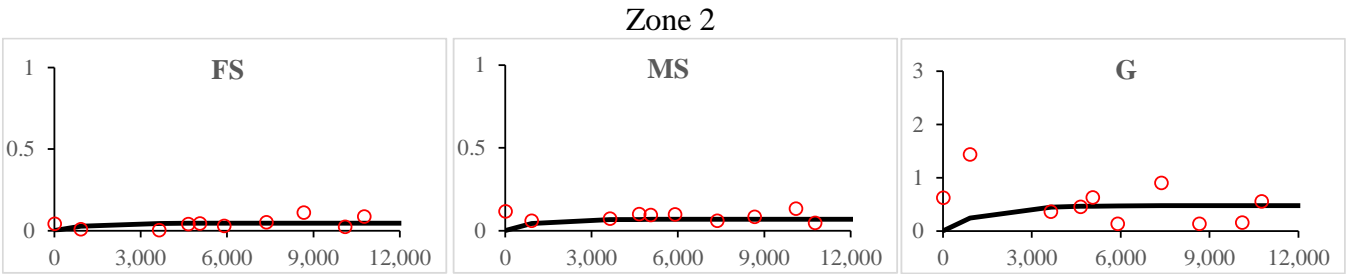
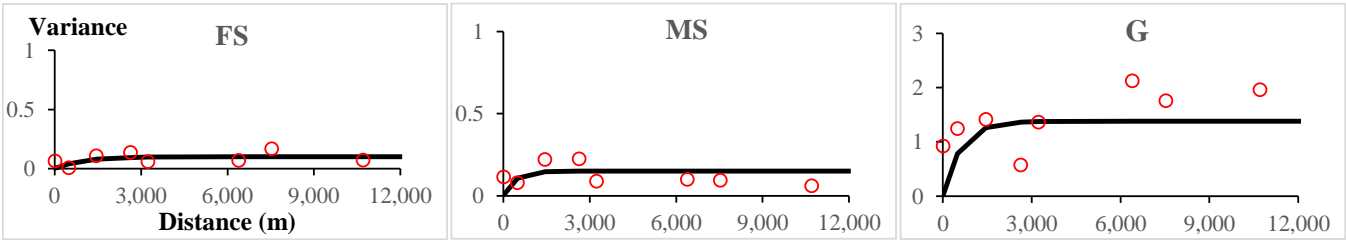
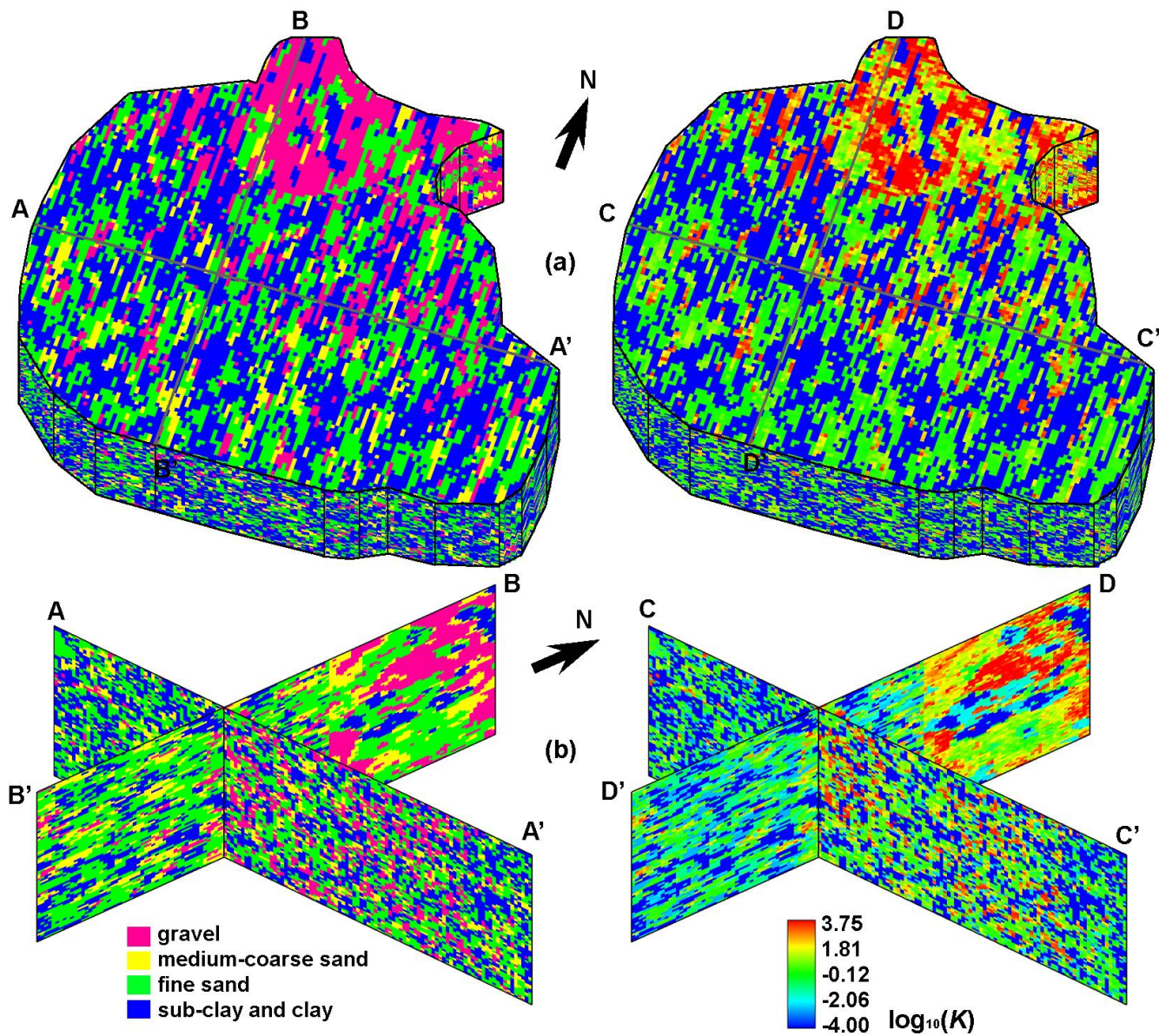


Figure 6





578 **Figure 7**



579

580